Tip-to-Tail Scramjet Simulation with Plasma-Assisted Control

Datta V. Gaitonde and Eswar Josyula
Air Force Research Laboratory, Air Vehicles Directorate (AFRL/VA), Computational Sciences Center, Wright-Patterson AFB, OH
{datta.gaitonde, eswar.josyul}@wpafb.af.mil

Abstract

A prominent pacing item in the quest for sustained hypersonic flight, and affordable access-to-space capability, is the development of an efficient air-breathing propulsion system. Key barriers of fluid dynamic origin includes, high thermal loads, shock/boundary layer interactions (SBLI) and fuel-air mixing at high-speeds, among other, all of which significantly degrade propulsion efficiency. One approach towards alleviating or eliminating these and other problems, and to provide a crucial energy management function, is to employ electromagnetic fields to control the relatively high temperature, low pressure environment encountered in proposed flight envelopes. To this end, several aspects of magnetogasdynamic (MGD) assisted scramjet flowpaths have been simulated using three-dimensional, integrated, multidisciplinary models requiring the large-scale resources available through the High Performance Computing Modernization Program (HPCMP). In this paper, we describe the complex flow field encountered in a scramjet and its control at various electromagnetic parameters. Among the key conclusions derived from these high-fidelity simulations are the limiting nature of separation and vortical structure formation on MGD generator operation and the deleterious effects of Hall currents, which induce non-intuitive system level asymmetries. Efforts have also focused on obtaining computationally intensive first-principles solutions for various high-temperature effects where phenomenological models have failed. Results from one of these, the modeling of detailed state-to-state kinetics of oxygen and nitrogen mixtures, is described, with emphasis on the derived insight into the phenomenon of vibrational freezing in nozzles, which is a key factor in loss of scramjet propulsion efficiency.

1. Introduction

Successful achievement of sustained hypersonic flight with air-breathing propulsion will have a profound impact on US military strategy and on commercial activity. Current Long Range Strike objectives call for technology development to "create desired effects anywhere on the globe within hours of tasking" with the ability to plan en route to the mission. Many technological advances remain to be realized before the conceptual design and evolution of vehicles can be matured to satisfy future environment drivers, which includes reduction in overseas presence, establishment of adversary exclusion zones, and affordable rapid response. Key among these are efficient and practical high-speed air-breathing propulsion systems, which can provide a unique means to rapidly deliver materiel and ordnance with high kinetic energy and lethality over large distances. Such systems will also serve dual-use purposes by providing a cost-effective method for routine, affordable access-to-space.

The harsh environment encountered by high-speed vehicles pose severe barriers, including catastrophically large structural and thermo-mechanical loads, and propulsion inefficiencies, which have not been overcome with current technologies. This has spurred the exploration of revolutionary leap-ahead technology advances to provide viable long-range strike and missile defense options for rapid global reach and responsive space access and control.

The revolutionary potential of electromagnetic interactions to alleviate or eliminate many pressing obstacles encountered in high-speed flight has led to a considerably renewed attention on these techniques. In principle, these methods can reduce local gradients, induce or suppress fluid dynamic bifurcations, or provide beneficial force and energy transfer between the fluid and the vehicle. In recent years, a number of system level thermodynamic studies have refined the feasible parameter space in which the desired objectives of

reducing thermo-mechanical loads and improving propulsion (typically scramjet) efficiencies maybe achieved. Several promising concepts have been vetted through these simple studies, and broad agreement has been reached on some specifics such as potential non-equilibrium ionization techniques, energy budgets and required magnetic field magnitudes[1,2]. However, many uncertainties persist on the physics of three-dimensional fluid-electromagnetic interactions, their scaling laws and optimal configuration details such as electrode design and placement. An unambiguous determination of engineering feasibility requires much additional difficult and expensive effort. One approach to reducing cost-risk associated with reproducing the rough environment in ground-test facilities is to supplement the exploration of potentially breakthrough concepts by applying new and self-consistent high-fidelity simulation tools which exploit modern computational facilities such as those provided by the DoD HPCMP.

The focus of the present effort is on tip-to-tail simulation of a scramjet operating under the magnetogasdynamic energy bypass procedure. A generic fully three-dimensional configuration is considered, as described in §2, specially designed to help examine the essential dynamics of scramjets. The fluid-plasma coupling requires care in both the theoretical formulation and numerical algorithm: a robust and efficient methodology is therefore employed as delineated in §3. The physics of operation are characterized, with and without MGD interaction, in §4. Emphasis is placed on aspects that are not easily amenable to experimental study i.e., the non-linear interplay between the fluid dynamics and plasma environment as well as on the complex, fundamentally multi-dimensional spatial relationships between the various fields. Although a significant element of phenomenological modeling has been employed in detailing the plasma environment, efforts have also focused on deriving the main high-temperature events from first principles. Since the effort requires the solution of massive equation sets, sub-configurations are considered. In §5, the complex issues associated with vibration-vibration energy interactions, and their effect on vibrational energy freezing in the nozzle are elucidated. The paper concludes by commenting on the significance of the present effort to the DoD (§6) and listing the specific systems used in this effort (§7).

2. Scramjet Configuration

The flowpath chosen for the simulation, Figure 1, starts from the underside of the air-vehicle, which serves as an external compression system. The inlet employs dual plane compression consisting of a vertical diffuser followed by a horizontal diffuser (*HD*). The pitch-plane shock from the ramp (8° angle) reflects off the cowl-lip, at which station sidewalls are assumed to start. The fuselage ramp terminates at the point where the shock reflected from the cowl-lip intersects the upper wall. The sidewalls of the *HD* are inclined at 4° to the freestream. The resulting swept spanwise shock waves facilitate the evolution of a highly three-dimensional flow at the entrance of the constant-area isolator, which starts where the crossing shocks (from inviscid estimates) reach the opposite walls. The isolator/combustor are represented by a constant area duct extending 4 streamwise distance units. A nozzle with 4° diverging wall angles for all but the lower surface (which does not diverge in order to provide a straight underside), serves to expand the flow. The nozzle side and bottom surfaces terminate where the width of the configuration equals that at the entrance: this facilitates the possibility of ganging such engines in a side-by-side fashion. The last component, the thrust surface, corresponds to an assumed underside of the vehicle of sufficient length to ensure that the flow is over-expanded at the exit of the computational domain. For the MGD-bypass procedure, a generator is mounted in the converging-sidewall inlet duct, with current being drawn through segmented electrodes. Theoretical considerations suggest that this procedure can reduce kinetic energy of the flow in the inlet through a more efficient procedure than if shock waves were employed for the same purpose, thus reducing distortion and losses, enhancing quality of flow for combustion and reducing the size of the inlet. The extracted energy may either be utilized for on-board purposes, or to accelerate fluid in the accelerator to enhance thrust. Such a device is also considered in Figure 1 in the expanding nozzle region downstream of the constant-area combustor.

3. Formulation and Numerical Procedure

In order to reduce uncertainty and computational load to a manageable level, a blend of first-principles and phenomenological elements is adopted. Thus, the low magnetic Reynolds number approximation ($R\sigma = \mu_m \sigma UL << 1$) is invoked based on the anticipated environment for MGD control in aerospace application. This permits the Navier-Stokes equations to be coupled to the Lorentz force and electromagnetic energetic terms through source terms. To facilitate solution of flows amenable to non-uniform mesh discretizations, a general curvilinear coordinate transformation is introduced, $x = x(\xi, \eta, \zeta)$, $y = y(\xi, \eta, \zeta)$, and $z = z(\xi, \eta, \zeta)$ and the governing equations take the form:

$$\frac{\partial \hat{X}}{\partial t} + \frac{\partial \hat{F}_I}{\partial \xi} + \frac{\partial \hat{G}_I}{\partial \eta} + \frac{\partial \hat{H}_I}{\partial \zeta} = \frac{\partial \hat{F}_V}{\partial \xi} + \frac{\partial \hat{G}_V}{\partial \eta} + \frac{\partial \hat{H}_V}{\partial \zeta} + \hat{S} \quad (1)$$

F_I, G_I, and H_I contain terms relevant to inviscid fluxes while F_V, G_V, and H_V include effects due to viscosity, and S is the source term containing effects of electromagnetic interaction with the flow. The various vectors of Eq. 1 have been detailed in References 3 and 4. The major non-dimensional parameters include the Reynolds number, $Re = \rho_{ref}U_{ref}L_{ref}/\mu_{ref}$, Mach number, M, Prandtl number, $Pr = \mu_{ref}C_p/k_{ref}$ and the interaction parameter $Q = \sigma_{ref}B_{ref}^2 L_{ref}/\left(\rho_{ref}U_{ref}\right)$.

The current vector, $\vec{j}$, is obtained from the phenomenological form of the generalized Ohm's law:

$$\vec{j} = \tilde{\tilde{\sigma}} \cdot \left[\vec{E} + \vec{U} \times \vec{B}\right] \tag{2}$$

Detailed expressions for the source terms as well as the conductivity tensor have been provided in Reference 5 and are not repeated here.

The electric field $\vec{E}$ is determined from the current continuity condition:

$$\nabla \cdot \vec{j} = 0 \tag{3}$$

which yields a Poisson equation. Introducing a scalar potential, $\vec{E} = -\nabla\phi$, the equation for φ is:

$$\nabla \cdot \left[\tilde{\tilde{\sigma}} \cdot [\nabla\phi]\right] = \nabla \cdot \left[\tilde{\tilde{\sigma}} \cdot \vec{U} \times \vec{B}\right] \tag{4}$$

In the present low R_σ approach, conventional high-resolution upwind-biased CFD techniques are straightforward to implement and have been incorporated together with a reconstruction method of nominally third order accuracy. Spatial discretization of the current continuity equation for the electric potential is accomplished with fourth-order compact differences. Complexities associated with shock waves and electrode-insulator junctures are addressed with a Pade-type filter.

All sets of equations for the fluid and turbulence quantities and the electric potential are integrated in time with the approximately-factored Beam-Warming-type method as described in Reference 5. By employing sub-iterations, tight coupling of the physical phenomena is ensured at the outer iteration level while the numerical advantages of fine-grain loose coupling are exploited at the inner iteration.

For the fluid dynamic variables, standard boundary conditions are prescribed. On all solid surfaces, the no-slip condition is enforced, the pressure gradient is assumed to be zero and the case-dependent wall temperature is specified. The downstream boundary, being predominantly supersonic is amenable to the zero gradient condition. At inflow boundaries, the flow vector is specified. Detailed conditions for the electric potential at insulators and electrodes have been described in Reference 6.

4. Scramjet Flowpath Analysis

The freestream flow parameters are assumed to be $M = 8$, $T_\infty = 250$K and $Re = 1.6 \times 10^6$. For an upstream width of $0.6m$, the reference velocity is $U_\infty = 2535.5m/s$. The plasma environment specification requires establishment of several parameters. The electrical conductivity, σ, is a strong function of the mechanisms producing ionization. Since ionization through the thermal dissociation path is likely to be small, especially in the generator, some kind of artificial enhancement method is required. Models of varying levels of sophistication have been developed for each method but introduce substantial computational load and require further validation before they may be applied to complex 3-D problems such as the one of interest. At present, we adopt elements of the phenomenology established in Reference 2 for e-beams.

The magnetic field is unperturbed by induced currents since the low R_σ approximation is invoked. The interaction of currents in the fluid with the external circuit, which is not simulated, occurs through four pairs of segmented electrodes mounted in the *HD* section to simulate the generator, with a similar arrangement in the nozzle for the accelerator (Figure 2). The potential gradients between the electrode surfaces are established from specified load factors and a local reference velocity through the relation, $K = (\Delta\varphi)/(wU_{local,ref}B)$, where φ is the potential on the electrode, w is the width of the channel at the mid-point of the electrode under consideration and U_{ref} is determined from the velocity profiles without plasma interaction. Specified electrode potentials, shown in Figure 2, vary with streamwise distance in a manner proportional to the width of the configuration.

Several calculations were made, spanning a wide range of interaction and Hall parameters. From these, only a few the most important conclusions are summarized below. The numerical method successfully reproduces all major aspects of the flow. For example, Figure 3 exhibits the shock structure along the horizontal midplane. Several discrete anticipated features are readily evident, including the intersection of the pitch plane compression shock reflected from the cowl lip. Sharp crossing shocks originating at the entrance to the *HD* become increasingly diffuse downstream as the flow becomes 3-D. The intersection of these shocks with the opposite sidewall boundary layer yields features of *SBLI* near the start of the isolator/combustor segment. The numerical procedure captures the subsequent shock and expansion train in a crisp fashion.

The interaction of shocks with the boundary layers developing on the upper and lower walls induces separation, which has a profound impact not only on the flow structure, but also on the operation of electromagnetic control. The existence of separation is

easily verified by examining the surface oil flow, shown for example on the lower surface in Figure 4. Lines of coalescence, indicative of separation, are formed near the sidewalls at the *HD* entrance and sweep spanwise towards the centerline, where they essentially merge. Lines of divergence, which are not as well defined by their nature, are formed near the corners and indicate flow attachment. A similar arrangement of surface oil flow is observed at the upper wall (not shown). 3-D streamlines separating at the line of coalescence lift off the surface and sweep spanwise in a spiraling motion to form a vertical structure, comprised of two counter-rotating cores. The sense of rotation of the left and right structures (looking downstream) is counter-clockwise and clockwise respectively. The net result is the development of low velocity vortical structures on the upper and lower walls, which essentially merge (see Figure 5) into a single coherent structure with two horizontally displaced lobes increasing in size as they progress downstream. Sidewall boundary layer thickness also increases as the fluid encounters the shock train. Smaller vortical structures are evident at each of the four corners of the duct. These "corner" vortices actually originate in the generator between the line of divergence and the sidewall but show more rapid growth in the combustor and the nozzle.

The non-uniformity arising from the complex fluid dynamic phenomena described above are reflected in the current, electric, and Lorentz force fields. To highlight points of interest, select current lines, shaded by magnitude, are shown in Figure 6 for the generator. The current is clearly highly 3-D and non-uniform with several unanticipated features. Chief among these is the formation of eddy currents—a consequence of the low-energy fluid in the separated region—and a concentration or "pinching" of current near the trailing edge of the generator. Also observed is boundary layer shorting: the computations suggest a possible method of suppressing this phenomenon by terminating the electrodes away from the upper and lower corners. The current patterns in the accelerator, as well as the electric field, are similarly interesting but are not discussed here. The electric field in the generator is relatively uniform in the interior, and is essentially oriented in the direction imposed by the electrodes. An interesting quirk however, is a reversal of the field direction at the electrode itself. The explanation for this is based on the vanishing velocity at the wall due to the no-slip condition. In this region, $\vec{U} \times \vec{B}$ is zero and the observed field reversal is essential to maintain the current direction and continuity. Since the current flows in the opposite direction in the accelerator, no such reversal is observed here. The body force field also shows non-intuitive behavior, with regions of reversal arising from the complex interaction of the velocity, magnetic, and current fields. This leads to an interesting observation that *MGD* generators may suppress separation by acting locally as accelerators.

The impact of MGD on the fluid consists of both body force and heating terms. Several analyses were conducted to determine efficiency in terms of energy extracted from the flow, Joule heating and work done by the flow (Figure 7). At the centerline, significant streamwise variation is evident in all quantities since the design does not facilitate the evolution of a spatially monotonic state. Although the effective load factor must approach unity under the present setup, the effect on the centerline is the opposite (reduced load factor) due to the current constriction observed in Figure 6a. Generator operation is observed to be relatively efficient: the largest component is the work done by the fluid and energy extracted from the flow $\vec{j} \cdot \vec{E}$ is larger in magnitude than the Joule heating term. The energetic interaction is smaller in the accelerator, where the granularity of the electrodes is more evident in the peaks, of which there is one per electrode. The reduction in effective load factor yields much smaller interaction near the third and fourth electrodes. Nonetheless, Joule heating focused locally near the centerline remains a small part of the energy input to the fluid. Although the efficiency of the generator is found to be relatively high, a length limitation arises if separation is encountered because of the above noted constriction.

Hall currents are likely to play an important role in the parameter space of hypersonic flight, which is characterized by relatively low electrical conductivity and high magnetic fields. Despite the use of a segmented electrode configuration, the Hall effect has a significant impact on the performance of MGD components. Two major effects observed are a development of asymmetry about the vertical plane and a significant modification of the vortical structures and their evolution. The vortical structure (Figure 8) is initiated in the same manner, through separation of the wall boundary layers. However, the upper and lower structures do not grow to encompass the height of the channel. Rather, they are compressed and are seen to move to the left of the centerline. The higher pressure on this side causes the sidewall boundary layer to separate. The result of this is most evident at the end of the combustor, where three structures on each of the upper, lower, and left sidewall are visible. Although not shown, the electromagnetic fields were also examined. The electric current orientation obtains a distinct downstream-oriented component, which in turn yields a substantial spanwise Lorentz force component. This is the source of the complex sequence of wave patterns that ultimately explain the features observed in Figure 8.

5. Vibrational Relaxation

The problem of vibrational non-equilibrium—specifically freezing of this energy mode—is of considerable interest in the performance of high-speed propulsion devices, since it represents an effective loss of thrust. Traditional approaches, based on simple theories coupled with substantial empiricisms have proven inaccurate for prediction in regions outside the immediate vicinity of the point of calibration. To surmount this limitation, the time-dependent Master equations are solved to account for energy exchanges of vibration-translation (V-T), vibration-vibration (V-V), dissociation and recombination. This method is computationally intensive because of the need to resolve multiple quantum levels, and is therefore utilized only on the nozzle sub-component. Some key findings are summarized in the context of Figure 9. Nozzle flows are characterized by a fall in translational temperatures along its length, which results in a large drop in the dissociation rates. However, the change in the recombination rate for this temperature drop is small, and the rates are higher than the dissociation rates. For such recombination-dominant flows, the role of vibrational population enhancement was evaluated under[7] thermal and chemical nonequilibrium conditions. This study revealed that the higher recombination rate leads to a population enhancement which increases along the nozzle length, with the highest enhancement at the exit of the nozzle. The effect of the enhancement is to reduce the effective recombination rate. These results are useful in the development of vibration-dissociation coupling models for computing hypersonic expanding nozzle flows under thermal and chemical nonequilibrium conditions.

6. Significance to DoD

USAF goals of accomplishing sustained hypersonic flight as an independent desirable, or to couple with the associated drive towards routine, on-demand, access-to-space are critically dependent on the development and utilization of revolutionary new technologies. Cost considerations demand the early incorporation of simulation and modeling in the development procedure. The present effort seeks to fulfill a part of this key requirement, by utilizing a state-of-the-art high-fidelity simulation of revolutionary plasma-based flow control to evolve sustained hypersonic flight through air-breathing scramjet propulsion.

The physics inherent in the problem is described by a highly multi-disciplinary equation set, including not only the coupled Navier-Stokes and Maxwell equations, but also models to represent ionization, thermal non-equilibrium and combustion. Solution of the large stiff equation set is greatly facilitated with state-of-the-art upwind and high-order Pade-type spatial discretizations, robust temporal advancement schemes and full exploitation of massively parallel systems. The goal of this on-going effort is to demonstrate this new, highly-accurate enabling technology to facilitate simulation-led development of scramjets utilizing advanced electromagnetic flow control concepts.

Although the specific goal of this proposal is a tip-to-tail scramjet calculation, it is important to recognize that the demonstration has profound impact on various other areas where plasma fluid interactions are important. This includes low-speed flow control methods, cooling of nuclear components with liquid metal flows and various biomedical applications. The utility of simulation scales directly with the realism of the model incorporated into the numerical procedure. The present approach deploys the most advanced high-fidelity numerical schemes to predict coupled aerospace plasma/fluid phenomena, and upon completion will demonstrate the cost efficiency of simulation-led design and development.

This DoD Challenge Project addresses science issues prior to and during the development phase of advanced technology demonstrations. Such an approach reduces development costs by a significant factor through vetting of inefficient and unworkable concepts and providing lessons-learned experience at minimal costs. Furthermore, by reducing the wall clock time, the massively parallel simulation strategy provides the versatility needed to foster the generation and testing of out-of-the-box concepts and to confront and overcome key physics-based limitations, thus precluding costly technological surprises at advanced stages of the program.

7. Systems Used

NAVO SP4, NAVO SP3, NAVO SV1, ASC SP3, ERDC CRAY X1, ERDC O3K

8. CTA

Computational Fluid Dynamics (CFD) 70% and Computational Electromagnetics and Acoustics (CEA) 30%

References

1. Kuranov, A., V. Kuchinsky, and E. Sheikin, "Scramjet with MHD Control under "AJAX" Concept. Requirements for MHD Systems." *AIAA Paper 2001-2881*, June 2001.

2. Macheret, S., M. Shneider, and R. Miles, "Magnetohydrodynamic Control of Hypersonic Flows and Scramjet Inlets Using Electron Beam Ionization." *AIAA J.*, Vol. 40, No. 1, Jan 2002, pp. 74–81.

3. Gaitonde, D., "Development of a Solver for 3-D Non-ideal Magnetogasdynamics." *AIAA Paper 99-3610*, June 1999.

4. Gaitonde, D. and J. Poggie, "Simulation of Magnetogasdynamic Flow Control Techniques." *AIAA Paper 20002326*, 2000.

5. Gaitonde, D. and J. Poggie, "An Implicit Technique for 3-D Turbulent MGD with the Generalized Ohm's Law." *AIAA Paper 2001-2736*, June 2001.

6. Gaitonde, D. and J. Poggie, "Elements of a Numerical Procedure for 3-D MGD Flow Control Analysis." *AIAA Paper 2002-0198*, Jan 2002.

7. Josyula, E. and W. Bailey, "Vibrational Population Enhancement in Non-equilibrium Dissociating Hypersonic Nozzle Flows." *J. Thermophys. Ht. Trans.*, (accepted for publication), 2004.

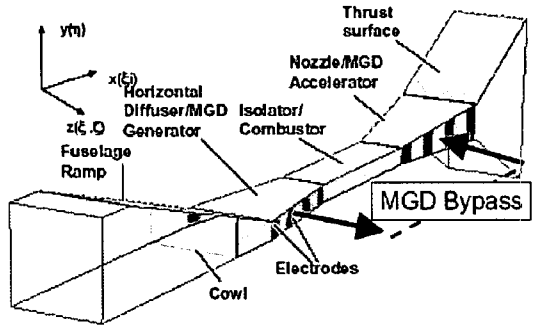

Figure 1. Simulated flow-through scramjet configuration

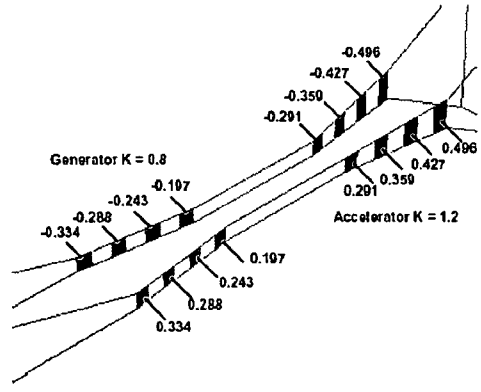

Figure 2. Electrode potentials in generator and accelerator

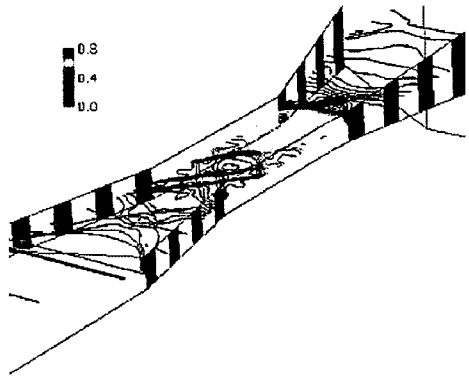

Figure 3. Pressure contours on horizontal mid-plane

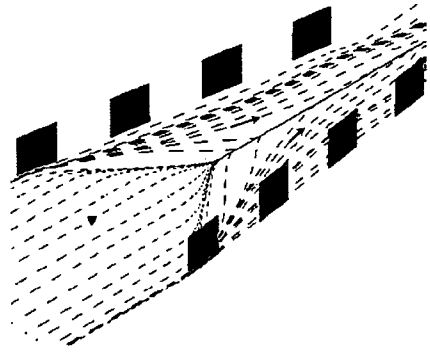

Figure 4. Simulated surface oil flow pattern on lower surface

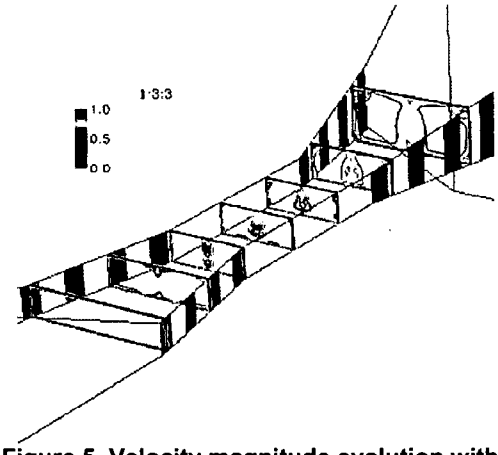

Figure 5. Velocity magnitude evolution with streamwise distance

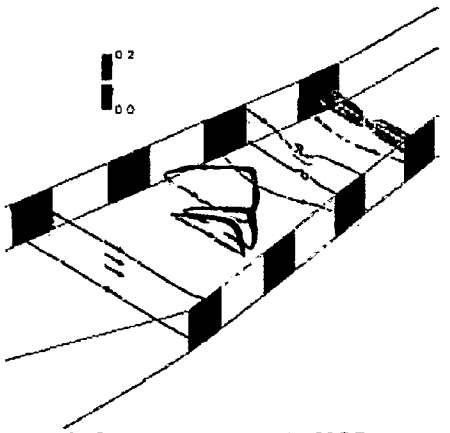

Figure 6. Current patterns in MGD generator

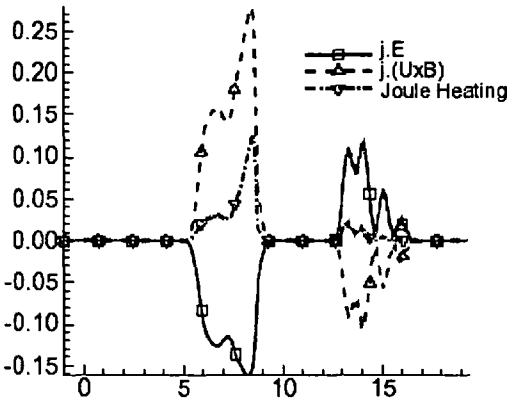

Figure 7. Breakout of energetic terms: Joule heating, work done and total

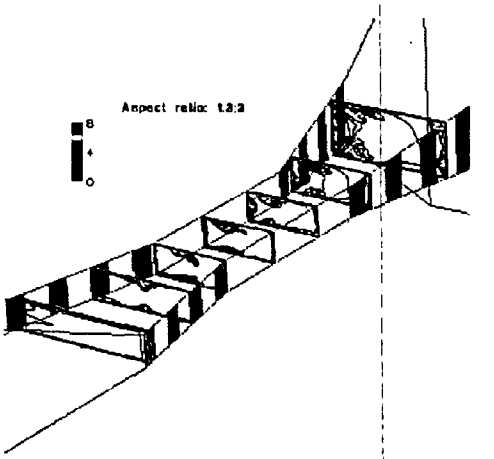

Figure 8. Effect of Hall currents on Mach contours

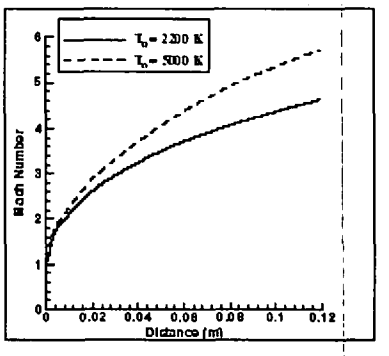

a) Mach number

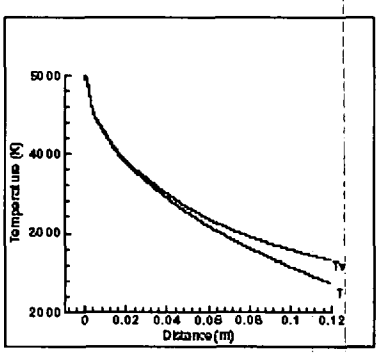

b) T and T_v

Figure 9. Nozzle flow phenomena